Anais da Academia Brasileira de Ciências
ISSN: 0001-3765
aabc@abc.org.br
Academia Brasileira de Ciências
Brasil

RODRIGUES, DIULIA C.Q.; SOARES JUNIOR, ATÍLIO P.; COSTA JUNIOR, ESLY F.; COSTA, ANDRÉA O.S.

Dynamic Analysis of the Temperature and the Concentration Profiles of an Industrial Rotary Kiln Used in Clinker Production

Anais da Academia Brasileira de Ciências, vol. 89, núm. 4, octubre-diciembre, 2017, pp. 3123-3136
Academia Brasileira de Ciências
Rio de Janeiro, Brasil

Anais da Academia Brasileira de Ciências (2017) 89(4): 3123-3136
(Annals of the Brazilian Academy of Sciences)
Printed version ISSN 0001-3765 / Online version ISSN 1678-2690
http://dx.doi.org/10.1590/0001-3765201720160661
www.scielo.br/aabc | www.fb.com/aabcjournal

Dynamic Analysis of the Temperature and the Concentration Profiles of an Industrial Rotary Kiln Used in Clinker Production

DIULIA C.Q. RODRIGUES[1], ATÍLIO P. SOARES JUNIOR[2], ESLY F. COSTA JUNIOR[3] and ANDRÉA O.S. COSTA[3]

[1]Programa de Engenharia Química, Universidade Federal do Espírito Santo/ UFES/ CCA, Campus de Alegre, Alto Universitário, s/n, Guararema, Caixa Postal 16, 29500-000 Alegre, ES, Brazil
[2]Fábrica de Cimento Nassau, Bairro Monte Líbano, 29300-970 Cachoeiro de Itapemirim, ES, Brazil
[3]Departamento de Engenharia Química, Escola de Engenharia, Universidade Federal de Minas Gerais, Avenida Antônio Carlos, 6627, 31270-901 Belo Horizonte, MG, Brazil

Manuscript received on September 30, 2016; accepted for publication on August 24, 2017

ABSTRACT

Cement is one of the most used building materials in the world. The process of cement production involves numerous and complex reactions that occur under different temperatures. Thus, there is great interest in the optimization of cement manufacturing. Clinker production is one of the main steps of cement production and it occurs inside the kiln. In this paper, the dry process of clinker production is analysed in a rotary kiln that operates in counter flow. The main phenomena involved in clinker production is as follows: free residual water evaporation of raw material, decomposition of magnesium carbonate, decarbonation, formation of C_3A and C_4AF, formation of dicalcium silicate, and formation of tricalcium silicate. The main objective of this study was to propose a mathematical model that realistically describes the temperature profile and the concentration of clinker components in a real rotary kiln. In addition, the influence of different speeds of inlet gas and solids in the system was analysed. The mathematical model is composed of partial differential equations. The model was implemented in Mathcad (available at CCA/UFES) and solved using industrial input data. The proposal model is satisfactory to describe the temperature and concentration profiles of a real rotary kiln.

Key words: Clinker, dynamic analysis, mathematical modelling, rotary kiln.

INTRODUCTION

Some of the challenges facing the cement industries are the high energy demand of production, the continuous increase in fuel prices, process complexity and environmental impact (Atmaca and Yumruta 2014, Tsamatsoulis 2014, Kaddatz et al. 2013, Gartner and Macphee 2011, Schneider et al. 2011, Mujumdara et al. 2007). To address these challenges, there is great interest in optimising the cement production process (Copertaro et al. 2015, Utlu et al. 2006).

The best-known type of cement is called Portland cement, which is defined as a hydraulic cluster that is basically obtained by grinding a mixture of clinker and gypsum (Copertaro et

Correspondence to: Diulia Caroline Quites Rodrigues
E-mail: diulaicaroline@hotmail.com

al. 2015). Thus, one of the main steps of the process for obtaining cement is the synthesis of the clinker (Atsonios et al. 2015, Saidur et al. 2011). Synthesis occurs inside the rotary kiln and involves complex physical (phase changes) and chemical (endothermic and exothermic reactions) processes (Lourenço et al. 2013, Saidur 2011, Silva 2007, Boateng and Barr 1996). The main clinker components are C_3S ($3CaO.SiO_2$), C_2S ($2CaO.SiO_2$), C_3A ($3CaO.AlO_3$) and C_4AF ($4CaO.Al_2O_3.Fe_2O_3$). The intermediate reactions for obtaining the clinker and their respective heats of reaction are shown in Table I, and the temperature ranges of the formation of chemicals are shown in Table II.

Clinker production can be performed in a dry or wet process (Paula 2009). On one hand, in the dry process, the mixture of agglomerates and aggregates are completely dried and ground to feed the kiln in powder form. On the other hand, in the wet process, the mixture is a mud that is fed into the kiln with approximately 30-40% of moisture (Saidur et al. 2011, Del Coz Díaz et al. 2002). This paper considers the dry clinker production, which is the most used process in Brazilian production of cement (Kihara and Visedo 2014).

A rotary kiln in a dry cement production can be divided into five zones (Stadler et al. 2011): heating zone, calcining zone, transition zone, firing zone and cooling zone. The position of the zones along the kiln depends on the temperature and the chemical reactions being performed in the solid (Spang 1972). The temperature profile along the rotary kiln is generally not directly measured due to the scarcity of sensors that supports its

TABLE I
Chemical reactions of the clinker production process (Paula 2009, Smith 2007).

Clinkerisation step	Chemical Reaction	Reaction heat (kJ/kg)
Evaporation of residual free water and water as a result of the clay combination	$H_2O(l) \rightarrow H_2O(v)$	+2443 (25°C)
Calcination	$CaCO_3(s) \leftrightarrow CaO(s) + CO_2(g)$	+1766 (20°C)
Magnesium carbonate decomposition	$MgCO_3(s) \rightarrow MgO(s) + CO_2(g)$	+1188 (20°C)
Formation of the liquid phase	$3CaO(s) + Al_2O_3(s) \rightarrow 3CaO.Al_2O_3(s)\ (C_3A)$ $4CaO(s) + Al_2O_3(s) + Fe_2O_3(s) \rightarrow 4CaO.Al_2O_3.Fe_2O_3(s)\ (C_4AF)$	-15 (20°C) -84 (20°C)
Formation of silicate dicalcium	$2CaO(s) + SiO_2(s) \rightarrow 2CaO.SiO_2(s)\ (C_2S)$	-717 (20°C)
Formation of tricalcium silicate	$3CaO(s) + SiO_2(s) \rightarrow 3CaO.SiO_2(s)\ (C_3S)$	-528 (20°C)

TABLE II
Temperatures of the chemical reactions of clinker production (Paula 2009).

Temperature	Chemical Reaction
Above 800°C	Start of the CaO manufacturing process
Between 800°C and 1200°C	Formation of C_2S
Between 1095°C and 1205°C	Formation of C_3A and C_4AF
Between 1260°C and 1455°C	Formation of C_3S from C_2S
Between 1455°C and 1300°C	Crystallisation of C_3A and the C_4AF liquid phase C_2S and C_3S silicate practically remain unchanged both in form and composition

internal operating conditions. Thus, estimating the temperature profile along the kiln is an important object of study.

In a previous work (Spang 1972), a dynamic model was developed. The model was composed of partial differential equations describing the mass balance and the system power (Spang 1972). The model is capable of predicting the concentration and temperature profiles along a rotary kiln operating in counterflow (Spang 1972). A flame model was also developed to quantify the amount of energy supplied to the system (Spang 1972). The equations that comprise this model (Equations 1 to 29) are presented in the Appendix. The results qualitatively describe the behavior of kilns, but the steady state was not reached.

In the present paper, an adaptation of the previous model is implemented to make it more realistic (Spang 1972). Using realistic values of the operational properties provided by a Brazilian company, the concentration and temperature profiles of a real rotary kiln used in the industrial production of the clinker is obtained.

CALCULATION PROCEDURES

Initially, a modification of the original model (Spang 1972) was performed to obtain a more realistic description of the temperature and concentration profiles of the clinker components along the rotary kiln.

In the originally proposed model (Spang 1972) the variation of gas temperature over time was not considered. To improve the description of the process, an adjustment was made in the gas energy balance (Equation 13 of the Appendix), which consisted of adding a term of gas temperature variation into the equation. In this way, Equation 13 was substituted by Equation 30.

$$A_g C_{pg} \rho_g v_g \left(\frac{\partial Tg}{\partial z}\right) = \beta_1 \left(T_w - T_g\right) + \beta_2 \left(T_s - T_g\right) - C_{pg} \rho_g A_g \left(\frac{\partial Tg}{\partial t}\right) + q_f \qquad (30)$$

$$T_g\left(L,t\right) = T_{gi}$$

The flame model originally described (Spang 1972) (Equations 17, 18 and 19 of the Appendix) was replaced by an amount of energy supplied to the kiln by the fuel combustion. These changes enable the industrial professional to use the model more directly. In this paper, the quantity of energy proposed for the fuel combustion is constant and equal to 326.7 kW/m (3.9×105 BTU/ft.h). This amount, adjusted by trial and error, approaches the values commonly used in industry. Thus, the new proposed model is composed of Equations 1-12, 14-16 and 20-30 as listed in the Appendix.

After adaptations, realistic values of the operational properties of the clinker production as reported by a Brazilian industrial plant were employed in the model. The composition of the raw material used in the industrial production of the clinker is shown in Table III. The values were normalized in relation to CaO (kg/kg). Other

TABLE III
Input composition of the raw material in the rotary kiln reported by industry.

Chemical Species	Normalized Composition in relation to CaO (kg/kg)
$CaCO_3$	1.6666
SiO_2	0.4849
Al_2O_3	0.1133
Fe_2O_3	0.0651
H_2O	0.0117

TABLE IV
Rotary kiln data reported by industry.

Variables	American Units	International System
Inlet gas temperature	1391.67 ºR	773.15 K
Radio of the kiln (r)	7.00 ft	2.15 m
Length of the kiln	295.28 ft	90.00 m
Outside radius (r2)	2.148 m	7.05 ft

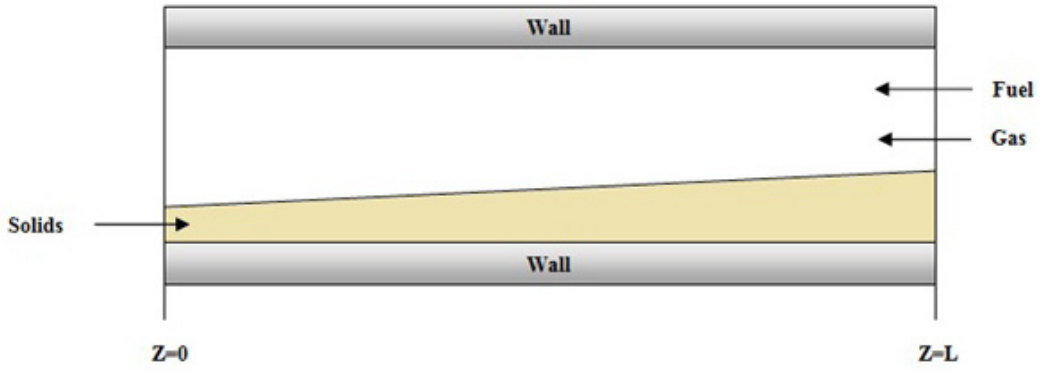

Figure 1 - Volume control used in the mathematical modelling of the rotary kiln (adapted from Spang 1972).

industrial operating properties employed in the model are shown in Table IV. The inner radius of the kiln was estimated to be 1.84 m (6.05 ft), the initial solid temperature, 562 ºR (312 K), and the initial temperature of the kiln wall, 662 ºR (367 K). These estimates were performed based on previous data (Spang 1972) and industrial realities.

The model was solved for different inlet speeds of gas and solid until the final composition of the clinker obtained in the simulation was similar to the actual values obtained in the cement industry (V). The best values for the gas and the solid inlet speeds were 274.32 m/s (-900 ft/hr) and 5.4864 m/s (18 ft/hr), respectively. Next, the temperature and concentration profiles obtained for the rotary kiln were analyzed considering these values.

For further analysis, the established inlet speed of gas and solid were varied as -20%, -10%, +10% and +20% to characterize the differences between the systems profiles. Subsequently, the obtained profiles were analyzed.

The model was solved using the discretization method for finite differences. Forty points of discretization were defined along the length of the rotary kiln. Discretization of the points was implemented according to the incoming stream of gas and solids into the kiln (Figure 1). For the discretization of the equations related to the solids, backward differentiation was used because they are fed into the beginning of the kiln (z = 0), and forward differentiation was used in the equations related to the gas because it is fed into the end of the kiln (z = L). The ordinary differential equations, functions of time, resulted from the discretization that were resolved by the numerical integrating method of Runge-Kutta with a variable step for error control, with an established tolerance of 10^{-7}. The model was implemented in Mathcad.

RESULTS AND DISCUSSION

Successive integrations were made in the model equations until the variations between the results

were no longer observed, which indicates achievement of the steady state of the rotary kiln. The temperature profiles of the gas, solid, and wall along the kiln's length in continuous operation are presented in Figure 2a. As expected, the kiln's temperature increases along its length to a maximum and then decays.

The $CaCO_3$ concentration profile along the length of the kiln is shown in Figure 2b. The profile follows the general pattern of a previous simulation (Spang 1972). Initially, there is a high concentration of $CaCO_3$ that decreases along the length of the kiln until it reaches zero.

The water concentration profile along the length of the kiln in steady state is shown in Figure 2c. The concentration of molecular water contained in the beginning of the feeding of solids decreases along the kiln until it becomes zero, as expected.

The concentration profiles of C_3S, C_2S, C_3A, C_4AF, and CaO along the length of the kiln in continuous operation are shown in Figure 2d. A decreasing behavior in the concentration of reactants followed by the formation of the clinker components is observed, which is in agreement with the expected.

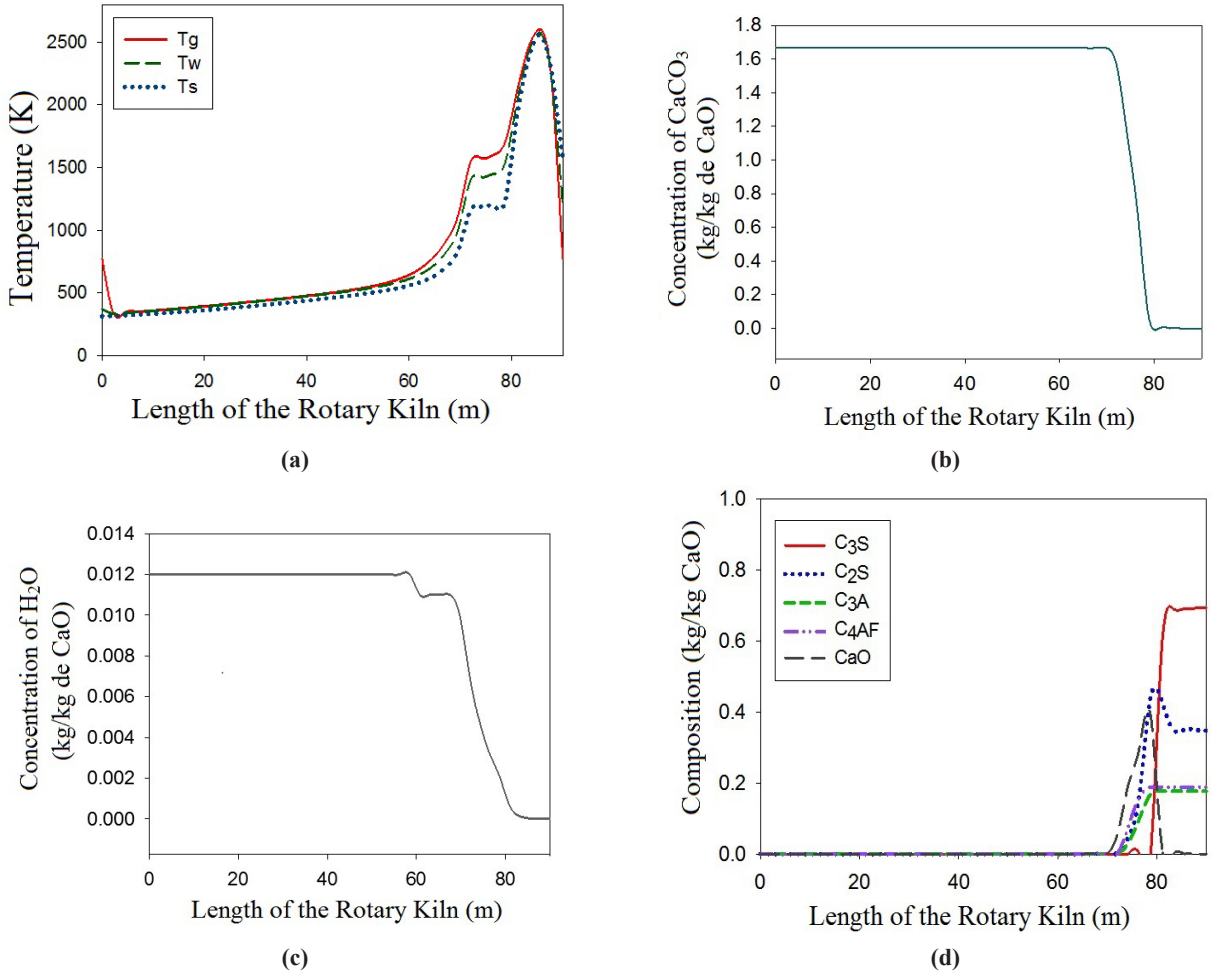

Figure 2 - Temperature profiles of the gas, the solid and the industrial rotary kiln's wall (**a**); concentration profiles of CaCO3 (**b**); concentration profiles of water (**c**) and concentration profiles of C3S, C2S, C3AF and CaO (**d**) in the industrial rotary kiln at steady state.

The clinker composition simulated by the model and the industrial clinker composition are presented in Table V. The final concentrations of the clinker components obtained by the model are relatively close to the actual concentrations of the cement industry. The $CaO.Al_2O_3$ and $12CaO.7Al_2O_3$ elements were not taken into consideration during modelling because they were not considered as part of the main elements of the clinker formation. The authors believe that this consideration caused the difference between the real (industrial composition) and the simulated composition of $3CaO.Al_2O_3$ presented in TableV.

Note that the final composition of the clinker widely varies from one industry to another and may vary even between operations of a same kiln because the composition of raw material is not constant, i.e., it may depend on the natural sources. In addition, changes in the operating conditions of a kiln produces variances in the final clinker concentration. An important aspect to highlight is that during the simulation of the actual system, it was not trivial to set values of inlet gas flow and solid flow that together satisfied the required values for the profiles of temperature and clinker concentration.

The profiles of temperature and clinker concentration obtained by varying the inlet gas speed by -20%, -10%, +10% and +20% are shown in Figures 3 and 4, respectively. The temperature profiles in Figure 3 are very similar, with only slight differences in the shapes of the temperature peaks noticed. In Figure 4, it is observed that C_3A, C_4AF and CaO have similar profiles in all of the proposed systems, whereas C_3S and C_2S have different profiles in each one of them. In general, the increase of the inlet gas speed from -20% to +10% increases the final concentration of C_3S and decreases the final concentration of C_2S. However, with +20% increase of inlet gas speed there is a decrease of the final concentration of C_3S and an increase of C_2S concentration.

As the quantity of energy proposed for the fuel combustion is constant, the increase of the inlet gas speed increases the energy transfer from the solid that is near the output of the kiln to the solid inside the equipment. The energy transfer is responsible for the increase of temperature inside the kiln, which is necessary for the chemical reactions to occur (Table II). The increase of the inlet gas speed from -20% to +10% increases the consumption of C_2S and the production of C_3S while CaO is available (Figure 4a, b and c). A +20% increase of the inlet gas speed strongly promotes the formation of C_2S, produced in lower temperatures than C_3S (Table II), and consequently reduces the availability of CaO in the system. Therefore, even with an increase of temperature, the production of C_3S is limited (Figure 4d).

The temperature and clinker concentration profiles that were obtained by varying the inlet solid speed by -20%, -10%, +10% and +20% are shown

TABLE V
Comparison of the results obtained by the model and the industrial composition of the clinker.

Chemical Species	Industrial Composition of the Clinker (mol/mol)	Simulated Composition of the Clinker (mol/mol)
$3CaO.SiO_2$	0.5600	0.4630
$2CaO.SiO_2$	0.2215	0.3074
$CaO.Al_2O_3$	0.0848	-
$12CaO.7Al_2O_3$	0.0087	-
$3CaO.Al_2O_3$	0.0816	0.1706
$4CaO.Al_2O_3.Fe_2O_3$	0.0433	0.0589
CaO	0.0000	0.0000
TOTAL	0.9999	0.9999

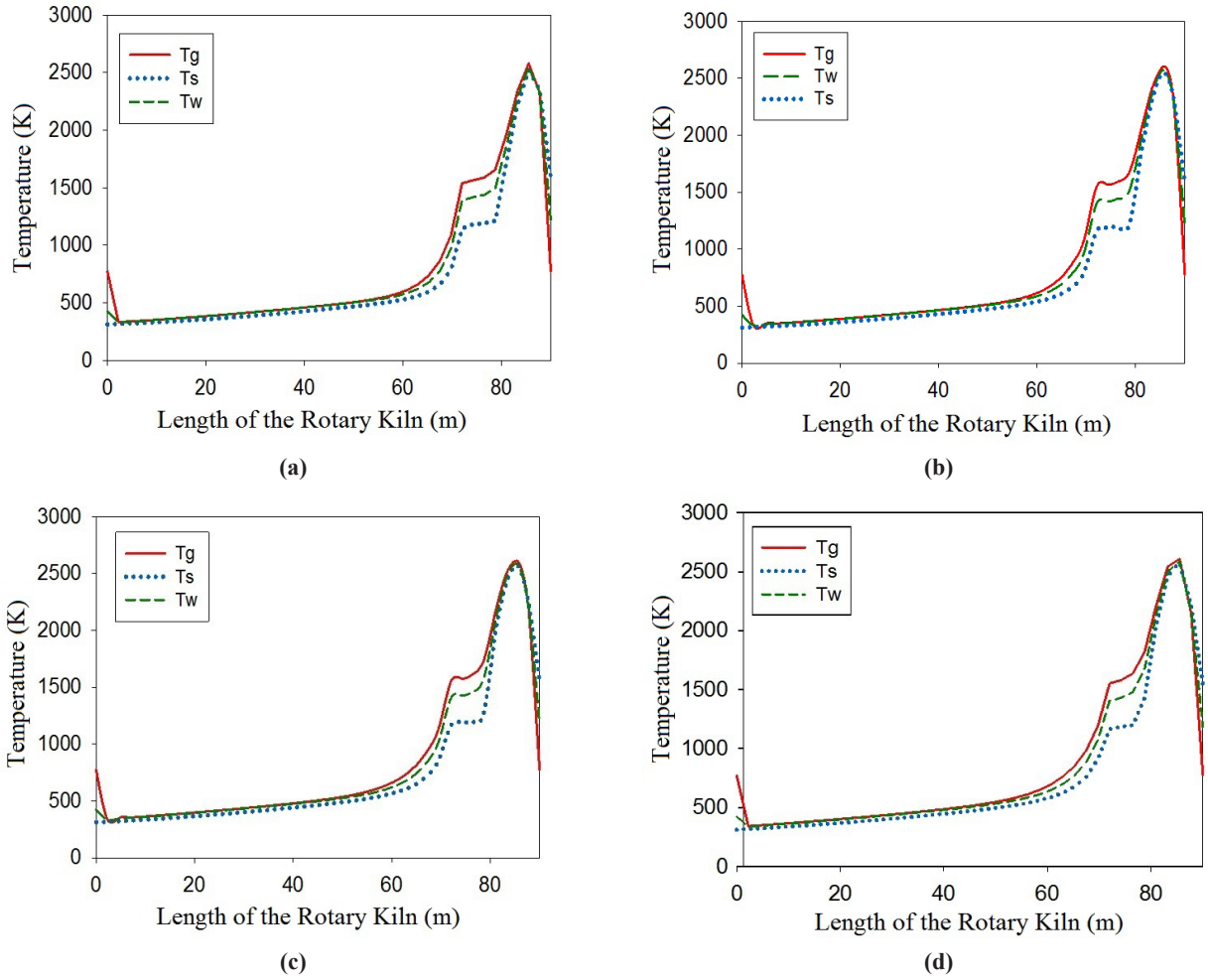

Figure 3 - Temperature profiles of the gas (Tg), the solid (Ts), and the wall (Tw) of the industrial rotary kiln at the steady state. (**a**) -20% of inlet gas speed; (**b**) -10% of inlet gas speed; (**c**) +10% of inlet gas speed; (**d**) +20% of inlet gas speed.

in Figures 5 and 6, respectively. In Figure 5, it is observed that the temperature of the burning zones, which correspond to the highest peak, decrease with the increase of the inlet solid speed. There is also an enlargement of the transition zone that corresponds to the second highest peak. In Figure 6, the concentrations of C_3A, C_4AF and CaO along the kiln have relatively similar profiles in all of the proposed systems, whereas C_3S and C_2S have different profiles in each one of them. The increase of the inlet solid speed promotes a later formation of C_3S through the length of the kiln and decrease in the C_3S final concentration. There is also an increase in the final concentration of C_2S.

As the formation of C_3A and C_4AF occurs before 1205°C (Table II), a reduction of temperature in the system (Figure 5) does not significantly affect the production of these species, which is not true for C_3S that are formed at higher temperatures (Table II). An increase of the inlet solid speed promotes a decrease of the temperature profile of the kiln and consequently reduces the formation of C_3S from C_2S, which occurs at temperature above 1260 °C (Figure 2). For this reason the profiles of C_3S and C_2S are modified.

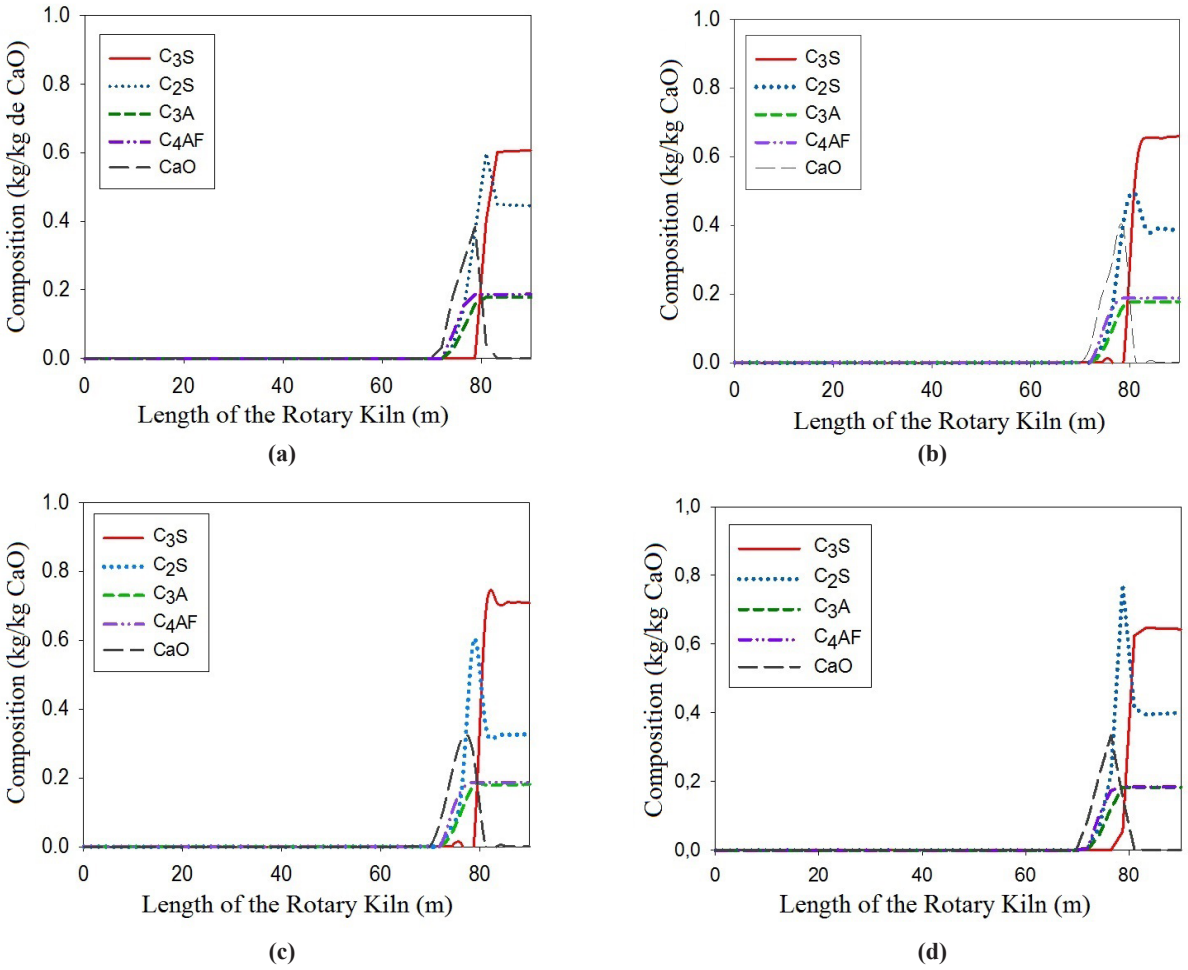

Figure 4 - Concentration profiles of C_3S, C_2S, C_3A, C_4AF and CaO in the industrial rotary kiln at steady state. (**a**) -20% of inlet solid speed; (**b**) -10% of inlet solid speed; (**c**) +10% of inlet solid speed; (**d**) +20% of inlet solid speed.

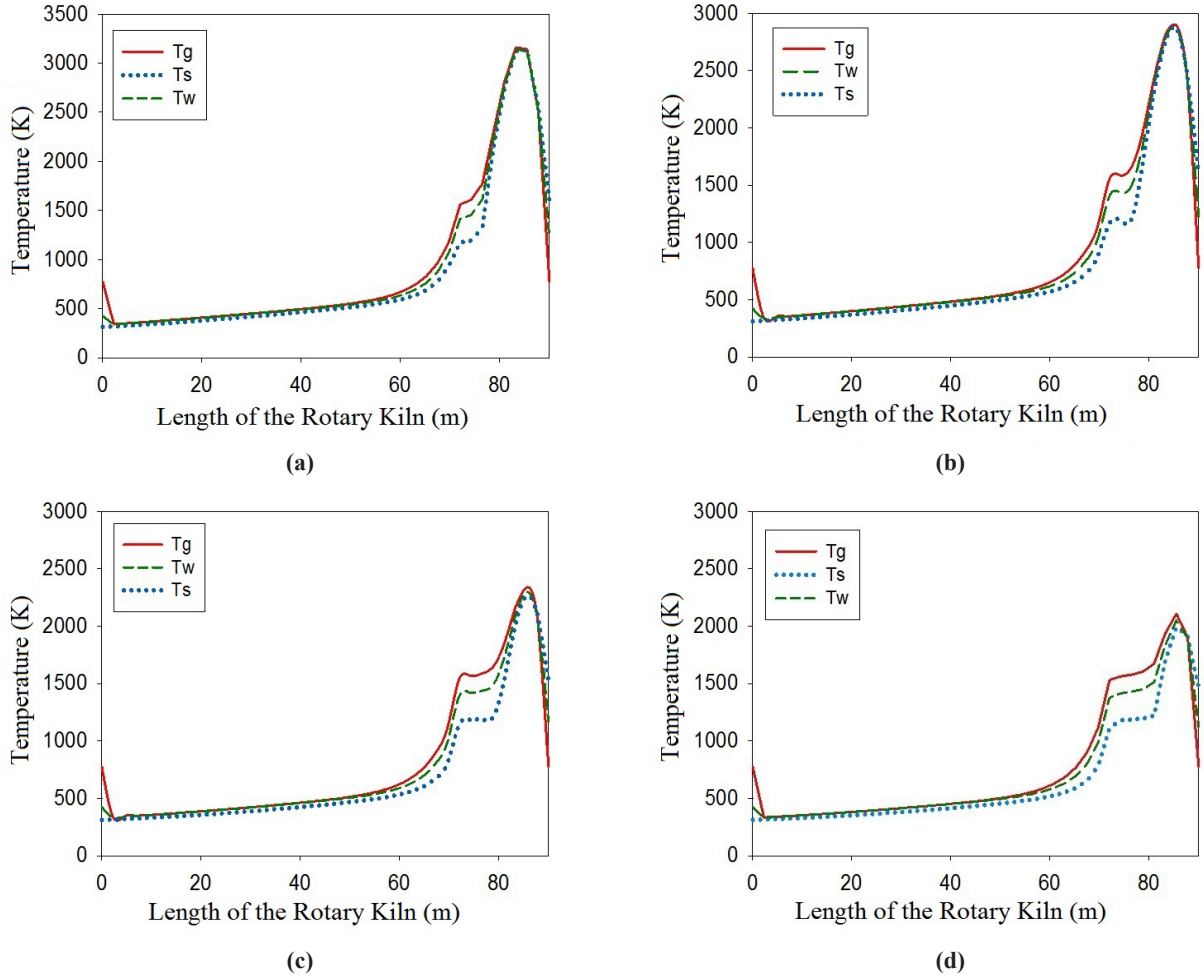

Figure 5 - Temperature profiles of the gas, the solid, and the wall of the industrial rotary kiln at steady state. (**a**) -20% of inlet solid speed; (**b**)-10% of inlet solid speed; (**c**) +10% of inlet solid speed; (**d**) +20% of inlet solid speed

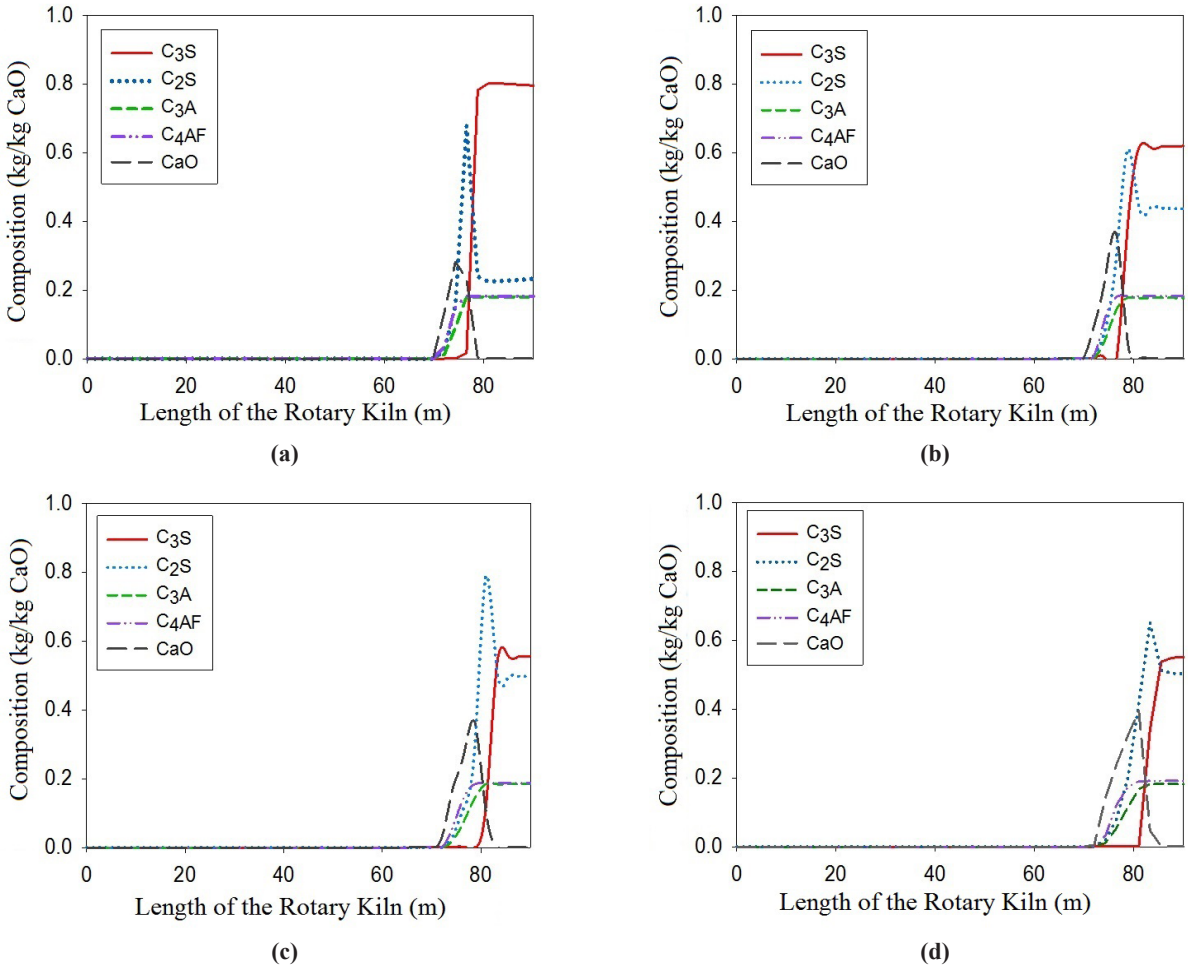

Figure 6 - Concentration profiles of C_3S, C_2S, C_3A, C_4AF and CaO in the industrial rotary kiln at steady state. (**a**) -20% of inlet gas speed; (**b**) -10% of inlet gas speed; (**c**) +10% of inlet gas speed; (**d**) +20% of inlet gas speed.

CONCLUSIONS

A mathematical model able to describe the temperature and concentration profiles of the clinker components along a real rotary kiln, in continuous operation, was developed. The mathematical model proposed in this paper does not require advanced computing to be solved, and it is easily adaptable to new industrial realities.

Variations of the gas and solid inlet speeds by -20%, -10%, +10% and +20% were individuality analysed according to the resulting temperature and concentration profiles of the clinker. These results were obtained via the model in the simulation of the real process. These parameters of operation were chosen because they have a significant influence in the process of cement production, and they can be changed without much modification in the kiln. In addition, these parameters can be used to find new operating conditions for the equipment.

NOMENCLATURE

	Notation	Value	Unit
f2	Coefficient of conduction – solid to gas	4	$(Btu/(h(ft)^2°F)$
f3	Coefficient of conduction – wall to solid	4	$(Btu/(h(ft)^2°F)$
f4	Coefficient of conduction – wall to outside air	0.7	$(Btu/(h(ft)^2°F)$
F	$\#Fe_2O_3/\ \#CaO$		
F_i	Initial value of $\#Fe_2O_3/\#CaO$	0.0469	#/#CaO
G_F	Amount of fuel per hour	53000	#/h
h_0	Fraction of radiation	0.0758	
K	Thermal conductivity of the wall	0.9	$(Btu/(h(ft)^2°F)$
K_f	Radiation rate – fuel		1/h
k_1	Radiation rate - $CaCO_3$		1/h
k_α	Radiation rate - C_3S		1/h
k_β	Radiation rate - C_2S		1/h
K γ	Radiation rate - C_3A		1/h
K δ	Radiation rate - C_4AF		1/h
K ω	Radiation rate – water		1/h
L	Total length of the kiln	400	ft
M	Depending on the subscript molecular weight of the chemicals		
$^{M}C_1$	Molecular weight of Carbon (C)		lb
P	Pressure		Btu/ft^2
P	Angle subtended by the surface of solid	3π/2	Radians
Qc	Heat generated by the chemical reactions		(Btu/(ft3 h))
qF	Heat generated by the fuel		(Btu/(ft h))
R	Ideal Gas constant	1.987	$Btu\,lbmol^{-1}\,R^{-1}$
Q	Heat generated or moving into a region		
r_F	Particle size of the fuel	10^{-2}	ft
r_1	Inside radius of the kiln	5	ft
r_2	Outside radius of the kiln	6	ft
r_3	Ratio of heat transfer in the chain section	5	ft

	Notation	Value	Unit
R ω	Reaction rate of water		$[h^{-1}]$
S	$\#SiO_2/\#CAO$		
S_i	Initial value of $\#SiO_2/\#CAO$	0.3398	# /#CAO
T_a	Temperature outside the kiln	561.7	°R
T_g	Temperature of the solid		°R
T_{gi}	Input temperature of the gas	1700	°R
T_s	Temperature of the solid		°R
T_{si}	Initial temperature of the solid	562	°R
T_w	Temperature of the wall		°R
v_g	Velocity of the gas	40000	ft/h
v_s	Velocity of the solid	-150	ft/h
Z	Distance along the kiln		ft
A	$\#C_3S/\#CAO$		
B	$\#C_2S/\#CAO$		
$\beta_1, \beta_2, \beta_3, \beta_4$	Heat transfer coefficient		(Btu/(h°R))
γ	$\#C_3A/\#CaO$		
δ	$\#C_4AF/\#CaO$		
ΔH_ξ	Heat of reaction - $CaCO_3$	1275	$Btu/\#CaCO_3$
ΔH_F	Heat of reaction – fuel	-14000	$Btu/\#CaCO_3$
ΔH_α	Heat of reaction - C_3S	11	$Btu/\#C_3S$
ΔH_β	Heat of reaction - C_2S	-381	$Btu/\#C_2S$
ΔH_ω	Heat of reaction – water	970	Btu/#water
ε_g	Radiation coefficient – gas	0.273	
ε_s	Radiation coefficient – solid	0.500	
ε_w	Radiation coefficient – wall	0.751	
ξ	$\#CaCO_3/\#CaO$		
ξ_i	Initial value of $\#CaCO_3/\#CaO$ at the input	1.784	#/#CaO
ρ_F	Density of the fuel		$\#/\#ft^3$
ρ_g	Density of the gas	0.05	$\#/\#ft^3$
ρ_s	Density of the solid	56	$\#/\#ft^3$
ρ_w	Density of the wall	112	$\#/\#ft^3$
Ψ	$\#CO_2/\#CaO$		
ω	#water/#CaO		
ω_i	Initial value of #water/#CaO	0.0649	#/#CaO

REFERENCES

ATMACA A AND YUMRUTA R. 2014. Analysis of the parameters affecting energy consumption of a rotary kiln in cement industry. Appl Therm Eng 66: 435-444.

ATSONIOS KP, GRAMMELIS SK, ANTIOHOS N, NIKOLOPOULOS E AND KAKARAS EM. 2015. Integration of calcium looping technology in existing cement plant for CO2 capture: Process modelling and technical considerations. Fuel 153: 210-223.

BOATENG AA AND BARR PV. 1996. A thermal model for the rotary kiln including heat transfer within the bed. Pergamon 39: 2131-2147.

COPERTARO E, CHIARIOTTI D, ESTUPINAN A, ALVARO N, PAONE B, PETERS GM AND REVEL A. 2015. discrete-continuous approach to describe $CaCO_3$

decarbonation in non-steady thermal conditions. Powder Technol 275: 131-138.

DEL COZ DÍAZ JJ, MAZÓNA F, RODRIGUES N, GARCÍA D AND SUÁREZ FJ. 2002. Design and finite element analysis of a wet cycle cement rotary kiln. Finite Elem Anal Des 39: 17-42.

GARTNER EM AND MACPHEE DE. 2011. A physico-chemical basis for novel cementitious binders. Cement Concrete Res 41: 736-749.

KADDATZ KT, RASUL MG AND AZAD R. 2013. Alternative fuels for use in cement kilns: process impact modelling. Procedia Engineering 56: 413-420.

KIHARA Y AND VISEDO G. 2014. A indústria do cimento e o desenvolvimento do Brasil. Associação Brasileira de Cimento Portland. Disponível em: <http://www.abcp.org.br/conteudo/imprensa/a-industria-do-cimento-e-o-desenvolvimento-do-brasil#.VQLvgo7F9NP>. Acesso em: 19/05/2015.

LOURENÇO RR, ANGÉLICA RS AND RODRIGUES JA. 2013. Preparation of refractory calcium aluminate cement using the sonochemical process. Mat Res 16: 731-739.

MUJUMDARA KSB, GANESHA KV, KULKARNIA SB AND RANADE VV. 2007. Rotary Cement Kiln Simulator (RoCKS): Integrated modeling of pre-heater, calciner, kiln and clinker cooler. Chem Eng Sci 69: 2590-2607.

PAULA LG. 2009. Análise termoeconômica do processo de produção de cimento Portland com co-processamento de misturas de resíduos, Brasil: Universidade Federal de Itajubá.

SAIDUR R, HOSSAINA MS, ISLAMA MR, FAYAZ H AND MOHAMMED HA. 2011. A review on kiln system modelling. Renew Sust Energ Rev 15: 2487-2500.

SCHNEIDER M, ROMER M, TSCHUDIN M AND BOLIO H. 2011. Sustainable cement production - present and future. Cement Concrete Res 41: 642-650.

SILVA MCC. 2007. Relações entre micestrutura, composição, resistência à ruptura e moabilidade de clínqueres de cimento Portland, Brazil: COPPE/UFRJ.

SMITH JM, VAN NESS HC AND ABBOTT MM. 2007. Introdução à termodinâmica da Engenharia Química, Rio de Janeiro: Ed. LTC, 644 p.

SPANG HA. 1972. A dynamic model of a cement kiln. Pergamon Press 8: 309-323.

STADLER KS, POLAND J AND GALLESTEY E. 2011. Model predictive control of a rotary cement kiln. Control Eng Pract 19: 1-9.

TSAMATSOULIS DC. 2014. Optimizing the control system of cement milling: process modeling and controller tuning based on loop shaping procedures and process simulations. Braz J Chem Eng 31: 155-170.

UTLU Z, SOGUT Z, HEPBASLI A AND OKTAY Z. 2006. Energy and exergy analyses of a raw mill in a cement production. Appl Therm Eng 26: 2479-2489.

APPENDIX

Material balance equations:

Water: $\frac{\partial \omega}{\partial t} = -R_\omega - v_s \frac{\partial \omega}{\partial z}$, $R_\omega = K_\omega \omega \omega \le 0.1 = \omega(0,t) = \omega_i K_\omega \omega > 0.1$

(1)

CO2: $\frac{\partial \Psi}{\partial t} = \frac{A_s}{A_g}\frac{\rho_s}{\rho_g}\frac{M_\Psi}{M_C} k_1 \xi - v_g \frac{\partial \Psi}{\partial z}$, $\Psi(L,t) = 0$ (2)

CaCO3: $\frac{\partial \xi}{\partial t} = -k_1 \xi \frac{M\xi}{M_C} - v_s \frac{\partial \xi}{\partial z}$, $\xi(0,t) = \xi_1$ (3)

C_3S: $\frac{\partial \alpha}{\partial t} = \frac{M\alpha}{M_C} k_\alpha (C)\beta - v_s \frac{\partial \alpha}{\partial z}$, $\alpha(0,t) = 0$ (4)

C_2S: $\frac{\partial \beta}{\partial t} = \frac{M\beta}{2M_C} k_\beta (C^2) S - \frac{M\beta}{M_C} k_\alpha (C)\beta - v_s \frac{\partial \beta}{\partial z}$, $\beta(0,t) = 0$ (5)

C_3A: $\frac{\partial \gamma}{\partial t} = \frac{M\gamma}{3M_C} k_\gamma (C^3) A - v_s \frac{\partial \gamma}{\partial z}$, $\gamma(0,t) = 0$ (6)

C_4AF: $\frac{\partial \delta}{\partial t} = \frac{M\delta}{4M_C} k_\delta (C^4) AF - v_s \frac{\partial \delta}{\partial z}$, $\delta(0,t) = 0$ (7)

Fe_2O_3: $\frac{\partial F}{\partial t} = -\frac{M_F}{4M_C} k_\delta (C^4) AF - v_s \frac{\partial F}{\partial z}$, $F(0,t) = F_i$ (8)

Al_2O_3: $\frac{\partial A}{\partial t} = -\frac{M_A}{4M_C} k_\delta (C^4) AF - \frac{M_A}{4M_C} k_\gamma (C^3) A - v_s \frac{\partial A}{\partial z}$, $A(0,t) = A_i$ (9)

SiO_2: $\frac{\partial S}{\partial t} = -\frac{M_S}{2M_C} k_\beta S (C^2) - v_s \frac{\partial S}{\partial z}$, $S(0,t) = S_i$ (10)

CaO: $\frac{\partial C}{\partial t} = -k_1 \xi - k_\alpha C\beta - k_\beta S(C^2) - k_\gamma C^3 A - k_\delta C^4 AF - v_s \frac{\partial C}{\partial z}$, $C(0,t) = 0$ (11)

Fuel (coal/oil): $\frac{\partial C_F}{\partial z} = \frac{1}{\rho_g v_g}\left[\frac{\Psi^M C_1 (PM_a)^2}{\rho_F M_{O_2} (RT_g)^2}\right] k_F d_0 C_F$, $C_F(L,t) = C_{F_i}$ (12)

Thermodynamic energy balance equations:

Gas: $A_g C_{pg} \rho_g v_g \left(\frac{\partial Tg}{\partial z}\right) = \beta_1 (T_w - T_g) + \beta_2 (T_s - T_g) + q_f$ (13)

$T_g(L,t) = T_{gi}$

Solid: $A_s C_{ps} \rho_s v_s \left(\frac{\partial Ts}{\partial z}\right) = \beta_2 (T_g - T_S) + \beta_3 (T_w - T_s) - C_{ps} \rho_s A_s \left(\frac{\partial Ts}{\partial t}\right) + A_s q_c$ (14)

$T_s(0,T) = T_{si}$

Kiln wall: $A_w C_{pw} \rho_w \left(\frac{\partial Tw}{\partial t}\right) = \beta_1 (T_g - T_W) + \beta_3 (T_S - T_W) + \beta_4 (T_a - T_W)$ (15)

Heat of reaction: $q_c = \frac{\rho_s}{(1+A_i+F_i+S_i)}\left[-\Delta H_\xi k_1 \xi - \Delta H_w R_w - \Delta H_\beta k_\beta S\left(C^2\right) - \Delta H_\alpha k_\alpha C\beta\right]$ (16)

Flame model: $q_f = \frac{G_f\left(-\Delta H_F\right)}{\left(p_g v_g\right)}\left[\frac{\Psi^M C_1 \left(PM_a\right)^2}{\rho_s M_{O_2}\left(RT_g\right)^2}\right] k_F d_0 C_F$ (17)

$$d_0 = 1 - \frac{k_F}{\left(\frac{D_0 3}{r_f^{\,2}}\right) + k_F} \quad (18)$$

$$D_0 = a_0 T_g^{\frac{3}{2}} \quad (19)$$

Reaction rate coefficient: $k_i = A_i \exp\left(\frac{-E_i}{RT_i}\right)$ (20)

i = 1, α, β,γ, δ, ω

$$k_F = \frac{3}{r_F} A_F \exp\left(\frac{-E_F}{RT_g}\right) \quad (21)$$

Coefficient of heat transfer:

$$\beta_1 = r_1 p\left[f_1 + 1.73x10^{-9}\left(1-h_0\right)\varepsilon_g \varepsilon_w \left(T_g^{\,2} + T_w^{\,2}\right)\left(T_g + T_w\right)\right] \quad (22)$$

$$\beta_2 = 2r_1 \sin\left(\frac{p}{2}\right)\left[f_2 + 1.73x10^{-9}\varepsilon_g \varepsilon_s \left(T_g^{\,2} + T_s^{\,2}\right)\left(T_g + T_s\right)\right] \quad (23)$$

$$\hat{a}_3 = r_1\left(2Ð - p\right)\left[f_3 + 1.73\ x10^{-9} h_0 \mathring{a}_w \mathring{a}_s \left(T_w^{\,2} + T_s^{\,2}\right)\left(T_w + T_s\right)\right] \quad (24)$$

$$\beta_4 = 2\Pi f_4 r_2 \quad (25)$$

$$h = 1 + \frac{2h_0 \sin\left(\frac{p}{2}\right)}{2\Pi - p} \quad (26)$$

Area coefficient:

$$A_g = \frac{r_1^2}{2}\left(p - \sin p\right) \quad (27)$$

$$A_s = \frac{r_1^2}{2}\left(2\Pi - p + \sin p\right) \quad (28)$$

$$A_w = 2\Pi\left(r_2^{\,2} - r_1^2\right) \quad (29)$$